Full Title:

Diffuse axonal injury predicts neurodegeneration after moderate-severe traumatic brain injury

Short title:

Diffuse axonal injury and neurodegeneration

Authors:

Graham NSN, Jolly A, Zimmerman K, Bourke NJ, Scott G, Cole JH, Schott JM, Sharp DJ

Neil SN Graham[1,2] http://orcid.org/0000-0002-0183-3368
Amy Jolly[1,2] http://orcid.org/0000-0002-7413-9772
Karl Zimmerman[1,2] https://orcid.org/0000-0003-1239-3414
Niall J Bourke[1,2] https://orcid.org/0000-0001-6478-1430
Gregory Scott[1,2] https://orcid.org/0000-0001-8063-5871
James H Cole[3 4] https://orcid.org/0000-0003-1908-5588
Jonathan M Schott[3] https://orcid.org/0000-0003-2059-024X
David J Sharp[1,2,5] http://orcid.org/0000-0003-4995-2240

Affiliations:

1. Department of Brain Sciences, Division of Medicine, Imperial College London
2. UK Dementia Research Institute, Centre for Care, Research and Technology
3. Dementia Research Centre, UCL Queen Square Institute of Neurology
4. Centre for Medical Image Computing, University College London
5. Centre for Injury Studies, Imperial College London

Word count: 4831
Display items: 8

Abstract

Traumatic brain injury is associated with elevated rates of neurodegenerative diseases such as Alzheimer's disease and Chronic Traumatic Encephalopathy. In experimental models, diffuse axonal injury triggers post-traumatic neurodegeneration, with axonal damage leading to Wallerian degeneration and toxic proteinopathies of amyloid and hyperphosphorylated tau. However, in humans the link between diffuse axonal injury and subsequent neurodegeneration has yet to be established. Here we test the hypothesis that the severity and location of diffuse axonal injury predicts the degree of progressive post-traumatic neurodegeneration. We investigated longitudinal changes in 55 patients in the chronic phase after moderate-severe traumatic brain injury and 19 healthy controls. Fractional anisotropy was calculated from diffusion tensor imaging as a measure of diffuse axonal injury. Jacobian determinant atrophy rates were calculated from serial volumetric T1 scans as a measure of measure post-traumatic neurodegeneration. We explored a range of potential predictors of longitudinal post-traumatic neurodegeneration and compared the variance in brain atrophy that they explained. Patients showed widespread evidence of diffuse axonal injury, with reductions of fractional anisotropy at baseline and follow-up in large parts of the white matter. No significant changes in fractional anisotropy over time were observed. In contrast, abnormally high rates of brain atrophy were seen in both the grey and white matter. The location and extent of diffuse axonal injury predicted the degree of brain atrophy: fractional anisotropy predicted progressive atrophy in both whole-brain and voxelwise analyses. The strongest relationships were seen in central white matter tracts, including the body of the corpus callosum, which are most commonly affected by diffuse axonal injury. Diffuse axonal injury predicted substantially more variability in white matter atrophy than other putative clinical or imaging measures, including baseline brain volume, age, clinical measures of injury severity and microbleeds (>50% for fractional anisotropy versus <5% for other measures). Grey matter atrophy was not predicted by diffuse axonal injury at baseline. In summary, diffusion MRI measures of diffuse axonal injury are a strong predictor of post-traumatic neurodegeneration. This supports a causal link between axonal injury and the progressive neurodegeneration that is commonly seen after moderate/severe traumatic brain injury but has been of uncertain aetiology. The assessment of diffuse axonal injury with diffusion MRI is likely to improve prognostic accuracy and help identify those at greatest neurodegenerative risk for inclusion in clinical treatment trials.

Keywords

TBI, Dementia, DAI, Head injury

Abbreviations

AD	Alzheimer's disease
APP	amyloid precursor protein
BACE-1	beta secretase
CTE	chronic traumatic encephalopathy
DAI	diffuse axonal injury
DARTEL	Diffeomorphic Anatomical Registration using Exponentiated Lie algebra
DTI	diffusion tensor imaging
FA	fractional anisotropy
FDR	false discovery rate
FLAIR	Fluid-attenuated inversion recovery
GCS	Glasgow coma scale
GM	grey matter
JD	Jacobian determinant
MNI	Montreal Neurological Institute
PS-1	presenilin 1
TBI	traumatic brain injury
WM	white matter

Introduction

Traumatic brain injury (TBI) is common, with worldwide annual incidence of 50 million and is associated with cognitive problems and dementia in survivors (Feigin *et al.*, 2013; Li *et al.*, 2017). TBI can trigger progressive neurodegeneration and is a risk factor for the development of Alzheimer's disease (AD), Parkinson's disease, motor neurone disease, chronic traumatic encephalopathy (CTE), with some risk elevation reported even after mild injury (McMillan *et al.*, 2011; Rosenfeld *et al.*, 2012; McMillan *et al.*, 2014; Li *et al.*, 2017; Graham and Sharp, 2019).

Experimental injury models implicate diffuse axonal injury (DAI) in causing neurodegeneration after traumatic brain injury. Neuronal loss over time may be a consequence of the axonal trauma leading to slowly progressive Wallerian degeneration (Povlishock and Katz, 2005), and/or a consequence of axonal damage promoting the development of progressive proteinopathies, leading to toxic damage and neuronal loss (Johnson *et al.*, 2010; Smith *et al.*, 2013; Tagge *et al.*, 2018). For example, traumatic cytoskeletal disruption produces axonal swelling and bulb formation, in which amyloid precursor protein (APP) accumulates with cleaving enzymes β secretase (BACE-1) and presenilin 1 (PS-1) to produce amyloid β (Johnson *et al.*, 2013b). Early pathologies of hyperphosphorylated tau (cis-P-tau) also arise as acute traumatic axonal damage promotes tau dissociation from microtubules, leading to aberrant phosphorylation, miscompartmentalisation and distal spread (Goldstein *et al.*, 2012; Kondo *et al.*, 2015; Tagge *et al.*, 2018). Progressive post-traumatic neurodegeneration may arise from prion-like propagation of traumatic proteinopathy distally; indeed animal models have demonstrated the transmissibility of tau generated in experimental injury (Zanier *et al.*, 2018). Further experimental work is awaited to replicate these findings, and to characterise the relative significance of spreading proteinopathy in post-traumatic neurodegeneration.

In humans, direct evidence for diffuse axonal injury triggering progressive neurodegeneration is lacking. However, neuroimaging tools are now available to estimate the location and severity of DAI as well as the extent of brain atrophy over time, allowing the hypothesis that patterns of injury predict the location and severity of subsequent atrophy to be tested. Patterns of DAI can be sensitively and accurately measured in vivo using diffusion MRI, providing a validated measure of post-traumatic axonal injury (Mac Donald *et al.*, 2007a; Mac Donald *et al.*, 2007b). Fractional anisotropy (FA) is the most widely used diffusion metric and provides a way to estimate white matter structure that is relatively stable in the chronic phase after TBI. Reduced FA is associated with axonal damage and surrounding inflammation (Mac Donald *et al.*, 2007a; Scott *et al.*, 2018) in addition to brain network dysfunction, poorer functional outcomes and

cognitive impairment particularly after moderate-severe injuries (Sidaros *et al.*, 2008; Bonnelle *et al.*, 2011; Kinnunen *et al.*, 2011).

Post-traumatic neurodegeneration typically involves the loss of tissue in grey and white matter but is particularly apparent in the degeneration of cerebral white matter first described in the 1950s (Strich, 1956; Smith *et al.*, 2013). This is commonly seen after moderate-severe TBI and can be accurately measured *in vivo* using changes in brain volume estimated from serial volumetric T1 MRI scans (Bobinski *et al.*, 2000; Cole *et al.*, 2018). Small changes in brain volume can be precisely measured using metrics such as the Jacobian determinant (JD) (Ashburner and Ridgway, 2012). We have previously reported loss of around 1.5% of the white matter per year in the chronic phase after TBI, which is dramatically increased relative to age-matched controls and similar to some neurodegenerative conditions (Cole *et al.*, 2018). High atrophy rates after TBI are associated with worse functional and cognitive outcomes, (MacKenzie *et al.*, 2002; Trivedi *et al.*, 2007; Bendlin *et al.*, 2008; Brezova *et al.*, 2014) with elevated longitudinal atrophy rates associated with poorer memory function (Ross *et al.*, 2012; Cole *et al.*, 2018). Progressive atrophy is seen for decades after moderate-severe TBI, with some evidence suggesting that atrophy rates can accelerate in some individuals over time (Cole *et al.*, 2015).

At present, there is limited information about the predictors of post-traumatic neurodegeneration, which we operationalise as atrophy over time. We have previously investigated a range of potential clinical and neuroimaging measures which have not reliably predicted white matter atrophy rates: these include the presence of focal lesions, severity measures such as lowest Glasgow Coma Scale (GCS), with only a small amount of variance explained by age at injury, or sex (Cole *et al.*, 2018). Diffusion abnormalities have previously been reported to be associated with reduced grey matter volumes in some post-injury settings (Warner *et al.*, 2010; Poudel *et al.*, 2020), but it remains uncertain how DAI relates to longitudinal atrophy rates in adult chronic moderate-severe TBI, particularly in white matter. In healthy middle-aged adults, DTI abnormalities have been associated with greater atrophy over time (Ly *et al.*, 2014). Assessment of DAI using MRI FLAIR, T2 and T2* sequences, rather than diffusion imaging, has been related to early progressive reduction in brainstem volume after moderate-severe TBI but not significant white matter volume change (Brezova *et al.*, 2014).

Here we test the following hypotheses: first, that fractional anisotropy (FA) at baseline scanning visit is related to progressive atrophy, quantified by the Jacobian determinant rate

(JD). We assess the relationship at the whole brain level and voxelwise to assess whether the location of DAI is the major determinant of subsequent neurodegeneration. We investigate the susceptibility of different white matter tracts to both axonal injury and neurodegeneration, and control for the potential impact of focal traumatic lesions. Furthermore, we assess the relative importance of different predictors of progressive neurodegeneration to establish the specificity of DTI measures of DAI, and test whether FA explains substantially more variance than these other factors.

Materials and Methods

55 patients were assessed after moderate-severe TBI, defined using the Mayo classification (Malec *et al.*, 2007) [mean age 42, standard deviation (SD) = 13; 45 males, 10 females]. Baseline MRI assessment was performed 3.5 years (mean) after injury, followed by a second MRI assessment 12.7 (mean) months later. (Table 1) Recruitment was via outpatient TBI clinics where patients were undergoing assessment neurological sequelae of injury. Inclusion criteria were age 18-80 and moderate-severe TBI. An injury was categorised as moderate-severe if any of the following criteria were satisfied: loss of consciousness ≥ 30 minutes, post-traumatic amnesia ≥ 24 hours, lowest Glasgow Coma Scale of < 13 (unless explained by another factor, eg. intoxication), evidence of contusion, intracerebral/subdural/extradural haematoma, subarachnoid haemorrhage, brainstem injury or injury penetrating the dura, (Malec *et al.*, 2007).

We excluded individuals with significant previous injury histories, major neurological or psychiatric issues (e.g. substance misuse) or contraindication to MRI. The cohort is a combination of patients recruited into a longitudinal study of outcomes after TBI, or more than one cross sectional study after TBI. We previously reported on post-traumatic neurodegeneration in many of this cohort (n=61 patients), a portion of whom were ineligible for the current study due to a lack of DTI MRI at the time of baseline scanning assessment (Cole *et al.*, 2018). All those who were eligible for inclusion in this study from our previous cohort were included, to minimise any selection bias.

Injury characteristics, such as lowest acute Glasgow Coma Scale (GCS), post traumatic amnesia (PTA) duration, and cause of injury were recorded. Post traumatic amnesia was defined by a combination of either prospective measurement in the acute phase post-injury, or

was retrospectively ascertained, where recovery the point at which the patient could consistently remember day-to-day events.

Healthy controls were screened according to the same exclusion criteria and were required to have no history of significant TBI. Recruitment was coordinated by local research facilities at the Hammersmith Hospital. All study participants provided written informed consent in accordance with the Declaration of Helsinki. Ethical approval was granted by the Hammersmith / Queen Charlotte's and Chelsea research ethics committee.

MRI acquisition

Imaging was acquired on two different scanners with minor differences in protocols: importantly, each individual's longitudinal imaging was performed on one scanner only. A Siemens 3T Verio (Siemens Healthcare) and Philips 3T Achieva (Philips Medical Systems) were used. High resolution T_1 volumetric assessment was performed at 3T on two separate occasions, using an MPRAGE sequence with voxel dimensions of 1 mm^3 on the Siemens scanner, and a T1-FE sequence with voxel dimensions of 1.2 x 0.9375 x 0.9375 mm on the Philips scanner. Further details can be found in the Supplementary data. Diffusion-weighted imaging was acquired on the two scanners in 64 directions. On the Siemens scanner, images were acquired along 64 non-colinear directions as previously described (Scott *et al.*, 2018). On the Philips scanner, diffusion-weighted images were in 4 runs of 16 non-colinear directions to give a total of 64 directions (see Supplementary) (Feeney *et al.*, 2017). FLAIR imaging was performed on both scanners, with gradient echo T2* and susceptibility weighted imaging performed on the Philips and Siemens scanners respectively to facilitate assessment of focal lesions.

Brain MRIs were examined by a neuroradiologist for lesions such contusions, haematomas or microbleeds using multiple imaging modalities at baseline, and lesion-masks were manually drawn for later analysis.

Neuropsychological testing

Neuropsychological testing was performed in the TBI group. An established battery of tests was administered during the studies comprising this dataset. To overcome multiple-comparisons issues, we analysed a previously defined subset of tests, sensitive to post-TBI deficits to limit multiple-comparisons issues (Cole *et al.*, 2018). These included the People Test

from the Doors and People Test (Baddeley *et al.*, 1994), whose score reflects associative learning and memory, choice reaction time, the trail making test, and matrix reasoning component of the Wechsler Abbreviated Scale of Intelligence Similarities (Wechsler, 1999).

Neuroimaging processing

Standard approaches were used for the DTI and volumetric processing (see Figure 1). Following acquisition (Figure 1A), diffusion images were processed using the FMRIB software library (version 5.0.8) (Kinnunen *et al.*, 2011), including distortion and eddy correction (Figure 1A). Tensor-based registration was performed using DTI-TK (Zhang *et al.*, 2007). Tensor images were normalised by bootstrapping volumes to the IXI aging template and then refining a group template using affine followed by non-linear diffeomorphic registration (Zhang *et al.*, 2007). Diffusion data were then registered to this template (group DTITK-space). An affine registration was performed to register the DTITK-space data to Montreal Neurological Institute (MNI) space using the FMRIB58 FA atlas. With the standard tract based spatial statistics approach the MNI-space mean fractional anisotropy (FA) image was thresholded at 0.2 to generate a white matter skeleton, and subject FA data projected onto the mean FA skeleton (FSL) (Smith *et al.*, 2006). Tract level data was generated using the Johns Hopkins University white matter atlas. The cingulum, fornices and tapetum were not included in ROI analyses due to poor sensitivity in these regions.

Volumetric analyses were performed as per (Cole *et al.*, 2018) using SPM 12 (UCL) (Figure 1B). T1 images were segmented into grey matter, white matter and CSF, and volumes of these tissue classes calculated at baseline and follow up scanning timepoints. Voxelwise longitudinal analysis was performed using the SPM 12 longitudinal registration tool, in which baseline and follow-up images are iteratively registered to produce a mid-point temporal average image (Ashburner and Ridgway, 2012; Cole *et al.*, 2018). The transformation necessary to move from the baseline to follow-up scan image is encoded by the Jacobian determinant (JD) representing the contraction or expansion necessary to warp each voxel to the temporal average. The JD is weighted by the interval between the two scans to give an annualised rate of change (the 'JD atrophy rate'). Since there is a JD for each voxel, a map of the brain can be readily visualised and further analysed. Annualised atrophy rates were calculated voxelwise, by taking an average of the JD values for each tissue class, such as grey or white matter, and within anatomical regions of interest defined by the Harvard-Oxford cortical and subcortical structural atlas (FSL). To facilitate registration to standard space, tissue specific JD maps were multiplied by the temporal average-space T1 images for each subject. A study-specific template was then

generated using the temporal average images of 20 randomly selected patients and controls using the SPM DARTEL non-linear registration (Diffeomorphic Anatomical Registration using Exponentiated Lie algebra) (Ashburner, 2007). Baseline, follow-up and individual average-space JD rate images were normalised to group space using DARTEL before affine registration to MNI space, with normalisation of volume and smoothing using an 8mm gaussian kernel.

Statistical analysis

Analyses were performed on volumetric and diffusion data as follows (Figure 1C). Wholebrain summary measures were calculated by adding grey and white matter tissue data. Volumes were normalised for participant head-size by dividing into total intracranial volume, defined as the sum of grey matter, white matter and CSF volume. FSL was used to generate mean and standard deviation (SD) values at each voxel within the healthy volunteer group. These maps were used to generate z-score maps for FA and JD for each patient and control by subtracting the control group mean map and dividing by the control SD map.

FSL Randomise software was used for voxelwise statistical analyses using the general linear model (Winkler *et al.*, 2014). These included scanner system (Philips versus Siemens MRI) and age as nuisance covariates, other than in the analysis of FA vs longitudinal atrophy rate in which only scanner system was included, based on hierarchical partitioning of the linear model (Supplementary Table A). FA maps were mean-centred for use as a voxelwise explanatory variable in Randomise, using Fslmaths. Multiple comparison correction was performed using permutation testing (10,000 permutations) and threshold-free cluster enhancement to generate maps of corrected P-values, thresholded to show only areas with $p<0.05$. One sided t-tests were done for the following comparisons between patients and controls, where there was strong a-priori evidence to do so: baseline volume differences, longitudinal atrophy rate differences, FA vs JD comparison after TBI. All voxelwise analysis was performed in MNI space to facilitate the comparison of volumetric and diffusion data.

To assess group differences of summary statistics, distributions were plotted and assessed visually for normality, with T tests used to compare group means where appropriate. Effect sizes for t tests were calculated to generate Cohen's d values and confidence intervals. Categorial variables were compared using the Chi-squared test. False discovery rate (FDR) correction was to address multiple comparisons issues for the battery of neuropsychological tests across multiple timepoints.

Data availability

The data underlying this study are available from the corresponding author on reasonable request.

Results

Diffuse axonal injury after traumatic brain injury

Following moderate-severe TBI the overall measure of white matter integrity, white matter FA, was lower than in controls at baseline (0.43 in patients vs. 0.47 in controls; $p<0.001$) and at follow-up scanning visit (0.43 vs. 0.47; $p<0.001$; see Table 2 and Figure 2A). Voxelwise comparison showed widespread reductions in FA throughout the white matter in patients compared to controls at baseline, particularly within large central white matter tracts such as the corpus callosum, superior and inferior longitudinal fasciculi, external capsules and posterior limbs of the internal capsules (Figure 2B). On summary measures (mean white matter FA), fractional anisotropy was stable over time in both patients and controls. Rates of change of FA did not differ significantly from zero in either patients or controls, nor were there significant differences in the rate of change in FA between the groups across the study duration.

Brain volume and increased atrophy rates after traumatic brain injury

White and grey matter volumes were significantly lower at baseline and follow-up after TBI compared with controls (All P values < 0.002, see Table 2). Atrophy over time, indicated by lower JD rate values, was significantly greater after TBI than in controls across white matter, grey matter and whole brain tissue classes (all P values <0.001, see Figure 3A). Voxelwise comparisons showed significant reductions in brain volumes cross-sectionally at baseline visit in patients versus healthy controls, involving a wide range of brain regions in both grey and white matter (Figure 3B). Furthermore, widespread regions of brain showed greater atrophy over time compared with controls on longitudinal voxelwise comparison (Figure 3C).

Diffuse axonal injury specifically predicts atrophy

As hypothesised (Figure 4A), there was a strong relationship between baseline diffusion MRI assessment of DAI and atrophy over time after TBI. Baseline FA predicted white matter atrophy rates (adjusted R^2 0.15, P=0.006, $\beta_{FA} = 0.26$) on multiple linear regression with scanner as a covariate. Wholebrain atrophy, including white matter areas, was predicted by FA (adjusted R^2 0.08, P=0.024). In contrast, grey matter atrophy (adjusted R^2 0.03, P=0.125) was not predicted by FA. GM region of interest analysis showed no significant correlation of FA and atrophy rates in cortical regions, or subcortical grey matter structures. In healthy controls,

no significant relationship was evident between baseline FA and atrophy in either the grey or white matter (p=0.609 in white matter, p=0.566 in grey matter). Group-level results are shown graphically in Figure 4B showing the predictor variable (FA) on the x-axis against the annualised atrophy rate on the y-axis. FA and JD are z-scored for simplicity of representation. Healthy controls (blue points) cluster around the origin with very little damage or progressive atrophy, while TBI patients occupy the lower-left quadrant of the figure, with considerable diffusion MRI evidence of DAI and elevated atrophy rates.

Areas with more diffusion evidence of DAI showed greater rates of atrophy over time. Voxelwise comparison of baseline FA and JD maps, excluding lesions on a per-subject basis, showed multiple regions with significant positive relationships (Figure 4C). These included parts of the corpus callosum, superior corona radiata bilaterally, internal capsules, posterior corona radiata and thalamic radiation on the left. There were no areas where there was a negative correlation between FA and JD. The strong correlation between FA and JD is shown for the peak voxel on voxelwise analysis, situated in the body of the corpus callosum (left side, MNI co-ordinates 106 85 99; Figure 4D).

The observed relationship was not driven by the presence of focal traumatic lesions. Around two thirds of our patients had some degree of focal brain abnormality produced by their injury such as contusions, gliosis or ex-vacuo dilatation. As expected, these most frequently involved the orbitofrontal regions, temporal poles, or occipital regions (supplementary Figure A). The group-level relationship between white matter damage and atrophy rates persisted when excluding lesioned voxels from each subject's mean FA / JD calculation (adjusted R^2 0.17, P=0.003, β_{FA} = 0.26). Notably, there was no significant correlation between lesion volume and white or grey matter JD atrophy rate.

White matter tracts with more evidence of diffuse axonal injury show greater atrophy over time

The relationship between baseline FA and atrophy rate (JD rate) was investigated for different white matter tracts. Tracts show differential susceptibility to DAI, so we hypothesised that those tracts showing more diffusion abnormalities would have greater atrophy over time. Across the whole group of patients there were varying degrees of diffusion abnormalities and atrophy rates (Figure 5). Tract FA and white matter JD measures were positively correlated (adjusted R^2 0.13, p=0.0117). Larger and more midline white matter structures, such as the

genu and body of the corpus callosum typically showed axonal damage and greater atrophy over time (Figure 5).

Diffuse axonal injury predicts atrophy over time better than other clinical or imaging measures

DAI severity and location explained far more of the variance in white matter atrophy than other potential biological factors. This was explored using hierarchical partitioning of a multiple linear regression model, which showed that baseline FA explained far more of the model's variance in white matter JD (53%) than any other biological influence. Age, sex, time since injury, lowest recorded Glasgow Coma Scale (GCS), the presence of microbleeds or volume of focal lesions on MRI all explained less than 5% of the variance in atrophy rates (Supplementary Table A). Surprisingly, baseline brain volume did not predict atrophy rates on either summary statistics or voxelwise (all $P>0.05$, including both grey and white matter tissue classes). The time interval between scans varied more in patients than controls, but was not significantly different between the groups, and did not relate to atrophy rates (Supplementary Figure B).

Higher brain atrophy rates are associated with poorer memory performance

We next explored the relationship between atrophy rates and levels of cognitive impairment. TBI patients showed impairment across a range of cognitive domains (Supplementary Table B). As we have reported previously, white and grey matter atrophy rates both correlated with a measure of memory performance (people test total score). In patients, atrophy rate across the study period related to the performance at the follow-up assessment (white matter JD $\rho = 0.53$, $p = 0.0005$; grey matter JD $\rho = 0.54$, $p = 0.0004$) (Figure 6).

Discussion

We show that diffuse axonal injury (DAI) measured by diffusion MRI strongly predicts brain atrophy following single moderate-severe traumatic brain injury (TBI). In the chronic phase after injury, white matter tract fractional anisotropy (FA) at baseline predicts the amount of volume loss seen in a white matter tract over time. We compared a number of factors that could influence neurodegeneration and DAI was by far the most important predictor. A majority of the variability in atrophy rates was explained by DAI. In contrast, less than 5% of the variance

in atrophy was predicted by any other hypothesised predictor, including clinical measures such as post traumatic amnesia and Glasgow Coma Scale, as well imaging measures of evidence of diffuse vascular injury and white matter volume at baseline. Lesion volumes did not relate to atrophy rates highlighting the importance of diffuse rather than focal traumatic damage. This provides evidence that DAI causes progressive neurodegeneration of white matter tracts, an effect that persists for many years after injury.

A causal link between DAI and axonal neurodegeneration is supported by experimental models of TBI, with rodent models of TBI producing a chronic and progressive degenerative process (Smith *et al.*, 1997; Tagge *et al.*, 2018). In humans, this degeneration is most prominent in the white matter (Cole *et al.*, 2018). Wallerian degeneration of damaged axons plays a role, particularly in the early phase after injury. This is the set of molecular and cellular events that clear degenerating axons and myelin from the central nervous system (CNS) (Vargas and Barres, 2007). Traumatic axonal injury produces degeneration of the axolemma and disintegration of the axonal cytoskeleton. This results in the disassembly of the microtubules, neurofilaments and other cytoskeletal component, resulting in fragmentation of the axon. In the peripheral nervous system Wallerian degeneration is a relatively rapid process. In CNS the degenerative process is much more chronic (Povlishock and Katz, 2005). The reasons for this discrepancy are not entirely clear, but may relate to the failure of CNS glial cells to fully clear myelin breakdown products, which are still seen in damaged white matter tracts many years after injury (Johnson *et al.*, 2013a). Future animal work combining MRI and histopathology could further investigate mechanisms and may explain some the spatial variability of FA and JD seen voxelwise, for example in the peak voxel where, though the trend strongly relates DAI and atrophy, a number of individuals had high atrophy rates but with positive zFA values, for reasons which are at present uncertain (Figure 4D).

Traumatic axonal injury can also trigger an active neurodegenerative process caused by toxic proteinopathies that are generated at the time of injury. Hyperphosphorylated tau and amyloid β pathology are generated within hours of injury and persist into the chronic phase. This pathology characterises many of the chronic neurodegenerative diseases associated with TBI, including CTE and AD (Smith *et al.*, 2013). The effects of biomechanical strain on axons can trigger the generation of hyperphosphorylated tau and amyloid β pathology. Cytoskeletal disruption caused by high strain leads to tau dissociation from microtubules, aberrant phosphorylation and possible trans-synaptic spread into other neurons (Zanier *et al.*, 2018). Amyloid pathology is also produced soon after injury. Axonal bulbs formed shortly after axonal damage provide an environment that accelerates the cleavage of amyloid precursor

protein to generate amyloid β (Gentleman *et al.*, 1993; Johnson *et al.*, 2013b). Hence, the generation and persistence of toxic proteinopathy in combination with gradual Wallerian-like degeneration of white matter tracts affected by TBI can explain the gradual white matter neurodegeneration associated with DAI (Hill *et al.*, 2016; Zanier *et al.*, 2018). Here, we operationalised neurodegeneration as progressive atrophy over time on volumetric T1 MRI but did not characterise the pathology underlying neurodegeneration, which could be explained by diverse mechanisms including slow Wallerian degeneration or various toxic proteinopathies. Ideally, one would fractionate post-TBI changes with evidence from other biomarkers, such as PET imaging, to classify injuries in a manner similar to the 'A/T/N' scheme in Alzheimer's disease, whereby amyloid (A) and tau (T) status are considered alongside MRI atrophy, denoting neurodegeneration (N) (Jack *et al.*, 2016).

We investigated the pattern and degree of axonal damage using diffusion MRI to measure FA. This is a sensitive marker of post-traumatic white matter abnormality (Mac Donald *et al.*, 2007a; Mac Donald *et al.*, 2007b). Widespread reductions in FA were seen in our TBI group, providing evidence for axonal injury affecting a large number of white matter tracts. Fractional anisotropy reductions are associated with disruption of white matter organisation, glial cell activation and myelin damage (Mac Donald *et al.*, 2007a; Scott *et al.*, 2018) and also predict the extent of brain network dysfunction, the degree of functional impairment and the pattern of cognitive impairment seen after TBI (Sidaros *et al.*, 2008; Bonnelle *et al.*, 2011; Kinnunen *et al.*, 2011). Hence, FA measures provide a clinically relevant imaging marker of axonal damage that characterises the early stages of Wallerian degeneration and neurodegeneration that is associated with the production of toxic proteinopathies. We did not find a relationship between white matter FA and progressive grey matter atrophy in our analyses. This may reflect a complex underlying relationship of DAI to grey matter volume change. Analyses may need to account for the location and extent of axonal injury, the connectivity of grey matter regions to areas of axonal injury, the extent of concomitant focal injury to grey matter regions, and a possible bidirectional relationship between white and grey matter damage and atrophy.

The key factor in determining the pattern of post-traumatic neurodegeneration is likely to be the biomechanics of the initial injury. DAI is caused by biomechanical forces exerted across white matter tracts at the time of injury (Gennarelli *et al.*, 1982). The distribution of these forces is likely to determine the spatial pattern of tract damage. Hence, the pattern of initial shear forces is key to understanding which white matter tracts are most likely to degenerate over time. Midline structures such as the corpus callosum are exposed to high shearing forces after many types of injury (Ghajari *et al.*, 2017). These tracts are particularly affected by DAI,

typically showing the most prominent diffusion MRI abnormalities and the most pronounced atrophy (Kinnunen *et al.*, 2011; Cole *et al.*, 2018). We have recently directly investigated the relationship between shear force, axonal injury and diffusion MRI abnormalities. We used a finite element model of a controlled cortical injury to predict the pattern of shear forces within the corpus callosum. These shear forces correlated with histopathological features of axonal injury and also the reduction of FA within damaged white matter. The results, which are in revision (Donat *et al.*, 2020), support a causal relationship between the biomechanics of an initial injury and axonal injury, which can be measured using diffusion MRI (Mac Donald *et al.*, 2007a; Tu *et al.*, 2016). In conjunction with this experimental work, our human results support a close relationship between initial biomechanical force, axonal injury and subsequent neurodegeneration. This is seen most clearly in tracts exposed to high shear forces such as the corpus callosum, where large abnormalities in FA are associated with high levels of tract degeneration. It is unclear whether our findings relating FA and atrophy would be seen after mild injuries, where brain volume change is far less pronounced (Cole *et al.*, 2015). It may be that white matter damage needs to exceed a threshold to give rise to significant progressive atrophy.

There are a number of potential limitations of our work. One concern is whether resolving oedema might confound the measurement of atrophy or microstructure after TBI. Although this is a potential confound in the acute stages following TBI, this is not an issue for our analysis as our participants are in the chronic phase post-TBI with a mean time since injury of 3.3 years. DTI is less sensitive to damage in regions with crossing fibres, thus increasing the chance of a type II error by adding noise into the observed relationship between damage and atrophy (Douglas *et al.*, 2015). We used a tract-based spatial statistics approach to DTI, where a 'skeletonised' map of axonal integrity is produced by sampling FA values from tract-centres, facilitating comparability between individuals by minimising noise due to registration errors. This approach has poorer sensitivity to damage at tract peripheries or indeed at grey/white matter boundaries (Smith *et al.*, 2006). A further potential confound is the effect of focal lesions and loss of brain tissue on estimates of microstructure and atrophy. We have carefully controlled for this issue by using an analysis pipeline that exclude focal injuries from our voxelwise analyses assessing DAI and atrophy correlations using lesion masking. Interestingly, we did not see significant frontal cortical differences in atrophy rates between patients and controls voxelwise (Figure 3C). This may relate to the specific spatial mechanics of injury within our patient group or perhaps the frontal-predominant distribution of focal lesions.

One potential limitation is the use of two different scanner systems for data acquisition. Although this introduces noise in the MRI measurements, we do not believe this affects any of our main findings. Importantly, each participant was scanned longitudinally on the same scanner, which dramatically reduces the impact of including two scanners. We also used hierarchical partitioning to systematically assess the impact of the two scanners on diffusion measures, which are particularly susceptible to different scanners. This showed that scanner system accounted for a significant amount of the explained variance in JD. Hence, scanner system was included as a nuisance covariate in analyses. Our control population was on average younger than the TBI patients. Although the difference did not reach statistical significance ($P = 0.053$) we cannot exclude an influence on between the group comparisons. As the central analysis relating DAI to atrophy rates is within TBI patients only however, this is not affected by any age difference. The time between TBI and the first study visit varied across our cohort, but was weighted towards first several years after injury. We found no significant correlation between time since injury and atrophy rates using linear regression across the group. However, a future investigation of larger numbers of patients spread over a very broad range of post-injury intervals would help to further characterise the temporal dynamics of DAI and progressive atrophy.

In summary, we report the novel finding that the extent and location of DAI predicts white matter degeneration after TBI. This is in line with experimental injury models showing that axonal damage triggers progressive neurodegeneration. This will lead to an improved ability to predict those at greatest neurodegenerative risk after TBI, which should improve outcome prediction and facilitate recruitment to clinical trials of anti-neurodegenerative and neuroprotective treatments (Schott *et al.*, 2010; Graham and Sharp, 2019).

Acknowledgements

This research was supported by an Alzheimer's Research UK Clinical Research Fellowship awarded to NG, and by the UK Dementia Research Institute (DRI) Care Research and Technology Centre (NG/DJS), an National Institute of Health Research (NIHR) Professorship (NIHR-RP-011-048) awarded to D.J.S. and by the NIHR Clinical Research Facility and Biomedical Research Centre (BRC) at Imperial College Healthcare NHS Trust. The research was also supported the Medical Research Council through a Clinician Scientist Fellowship awarded to D.J.S. J.M.S. acknowledges the support of the National Institute for Health Research University College London Hospitals Biomedical Research Centre, Wolfson Foundation, ARUK (ARUK-PG2017-1946), Brain Research UK (UCC14191), Weston Brain Institute (UB170045), Medical Research Council, British Heart Foundation and European

Union’s Horizon 2020 research and innovation programme (Grant 666992). G.S. was supported by an NIHR Clinical Lectureship (CL-2016-21-005). JC is funded by a UKRI Innovation Fellowship. The authors would like to thank the participants in this research project.

Competing interests

The authors declare that they have no competing interests.

References

Ashburner J. A fast diffeomorphic image registration algorithm. Neuroimage 2007; 38(1): 95-113.

Ashburner J, Ridgway GR. Symmetric diffeomorphic modeling of longitudinal structural MRI. Front Neurosci 2012; 6: 197.

Baddeley A, Emslie H, Nimmo-Smith I. Doors and people test: a test of visual and verbal recall and recognition. Bury St. Edmunds: Thames Valley Test Company; 1994.

Bendlin BB, Ries ML, Lazar M, Alexander AL, Dempsey RJ, Rowley HA*, et al.* Longitudinal changes in patients with traumatic brain injury assessed with diffusion-tensor and volumetric imaging. Neuroimage 2008; 42(2): 503-14.

Bobinski M, de Leon MJ, Wegiel J, Desanti S, Convit A, Saint Louis LA*, et al.* The histological validation of post mortem magnetic resonance imaging-determined hippocampal volume in Alzheimer's disease. Neuroscience 2000; 95(3): 721-5.

Bonnelle V, Leech R, Kinnunen KM, Ham TE, Beckmann CF, De Boissezon X*, et al.* Default mode network connectivity predicts sustained attention deficits after traumatic brain injury. J Neurosci 2011; 31(38): 13442-51.

Brezova V, Moen KG, Skandsen T, Vik A, Brewer JB, Salvesen O*, et al.* Prospective longitudinal MRI study of brain volumes and diffusion changes during the first year after moderate to severe traumatic brain injury. Neuroimage Clin 2014; 5: 128-40.

Cole JH, Jolly A, de Simoni S, Bourke N, Patel MC, Scott G*, et al.* Spatial patterns of progressive brain volume loss after moderate-severe traumatic brain injury. Brain 2018; 141(3): 822-36.

Cole JH, Leech R, Sharp DJ, Alzheimer's Disease Neuroimaging I. Prediction of brain age suggests accelerated atrophy after traumatic brain injury. Ann Neurol 2015; 77(4): 571-81.

Donat CK, Yanez-Lopez M, Sastre M, Baxan N, Goldfinger M, Seeamber R*, et al.* From biomechanics to pathology: predicting axonal injury from patterns of strain after traumatic brain injury. (in submission at Brain) 2020.

Douglas DB, Iv M, Douglas PK, Anderson A, Vos SB, Bammer R*, et al.* Diffusion Tensor Imaging of TBI: Potentials and Challenges. Top Magn Reson Imaging 2015; 24(5): 241-51.

Feeney C, Sharp DJ, Hellyer PJ, Jolly AE, Cole JH, Scott G*, et al.* Serum insulin-like growth factor-I levels are associated with improved white matter recovery after traumatic brain injury. Ann Neurol 2017; 82(1): 30-43.

Feigin VL, Theadom A, Barker-Collo S, Starkey NJ, McPherson K, Kahan M*, et al.* Incidence of traumatic brain injury in New Zealand: a population-based study. Lancet Neurol 2013; 12(1): 53-64.

Gennarelli TA, Thibault LE, Adams JH, Graham DI, Thompson CJ, Marcincin RP. Diffuse axonal injury and traumatic coma in the primate. Ann Neurol 1982; 12(6): 564-74.

Gentleman SM, Nash MJ, Sweeting CJ, Graham DI, Roberts GW. Beta-Amyloid Precursor Protein (Beta-App) as a Marker for Axonal Injury after Head-Injury. Neurosci Lett 1993; 160(2): 139-44.

Ghajari M, Hellyer PJ, Sharp DJ. Computational modelling of traumatic brain injury predicts the location of chronic traumatic encephalopathy pathology. Brain 2017; 140(2): 333-43.

Goldstein LE, Fisher AM, Tagge CA, Zhang XL, Velisek L, Sullivan JA*, et al.* Chronic traumatic encephalopathy in blast-exposed military veterans and a blast neurotrauma mouse model. Sci Transl Med 2012; 4(134): 134ra60.

Graham NS, Sharp DJ. Understanding neurodegeneration after traumatic brain injury: from mechanisms to clinical trials in dementia. J Neurol Neurosurg Psychiatry 2019.

Hill CS, Coleman MP, Menon DK. Traumatic Axonal Injury: Mechanisms and Translational Opportunities. Trends in neurosciences 2016; 39(5): 311-24.
Jack CR, Jr., Bennett DA, Blennow K, Carrillo MC, Feldman HH, Frisoni GB*, et al.* A/T/N: An unbiased descriptive classification scheme for Alzheimer disease biomarkers. Neurology 2016; 87(5): 539-47.
Johnson VE, Stewart JE, Begbie FD, Trojanowski JQ, Smith DH, Stewart W. Inflammation and white matter degeneration persist for years after a single traumatic brain injury. Brain 2013a; 136(Pt 1): 28-42.
Johnson VE, Stewart W, Smith DH. Traumatic brain injury and amyloid-β pathology: a link to Alzheimer's disease? Nature Reviews Neuroscience 2010; 11(5): 361-70.
Johnson VE, Stewart W, Smith DH. Axonal pathology in traumatic brain injury. Experimental neurology 2013b; 246: 35-43.
Kinnunen KM, Greenwood R, Powell JH, Leech R, Hawkins PC, Bonnelle V*, et al.* White matter damage and cognitive impairment after traumatic brain injury. Brain 2011; 134(Pt 2): 449-63.
Kondo A, Shahpasand K, Mannix R, Qiu J, Moncaster J, Chen CH*, et al.* Antibody against early driver of neurodegeneration cis P-tau blocks brain injury and tauopathy. Nature 2015; 523(7561): 431-6.
Li Y, Li Y, Li X, Zhang S, Zhao J, Zhu X*, et al.* Head Injury as a Risk Factor for Dementia and Alzheimer's Disease: A Systematic Review and Meta-Analysis of 32 Observational Studies. PLoS One 2017; 12(1): e0169650.
Ly M, Canu E, Xu GF, Oh J, McLaren DG, Dowling NM*, et al.* Midlife measurements of white matter microstructure predict subsequent regional white matter atrophy in healthy adults. Hum Brain Mapp 2014; 35(5): 2044-54.
Mac Donald CL, Dikranian K, Bayly P, Holtzman D, Brody D. Diffusion Tensor Imaging Reliably Detects Experimental Traumatic Axonal Injury and Indicates Approximate Time of Injury. The Journal of Neuroscience 2007a; 27(44): 11869.
Mac Donald CL, Dikranian K, Song SK, Bayly PV, Holtzman DM, Brody DL. Detection of traumatic axonal injury with diffusion tensor imaging in a mouse model of traumatic brain injury. Exp Neurol 2007b; 205(1): 116-31.
MacKenzie JD, Siddiqi F, Babb JS, Bagley LJ, Mannon LJ, Sinson GP*, et al.* Brain atrophy in mild or moderate traumatic brain injury: a longitudinal quantitative analysis. AJNR Am J Neuroradiol 2002; 23(9): 1509-15.
Malec JF, Brown AW, Leibson CL, Flaada JT, Mandrekar JN, Diehl NN*, et al.* The mayo classification system for traumatic brain injury severity. J Neurotrauma 2007; 24(9): 1417-24.
McMillan TM, Teasdale GM, Weir CJ, Stewart E. Death after head injury: the 13 year outcome of a case control study. J Neurol Neurosurg Psychiatry 2011; 82(8): 931-5.
McMillan TM, Weir CJ, Wainman-Lefley J. Mortality and morbidity 15 years after hospital admission with mild head injury: a prospective case-controlled population study. J Neurol Neurosurg Psychiatry 2014; 85(11): 1214-20.
Poudel GR, Dominguez DJ, Verhelst H, Vander Linden C, Deblaere K, Jones DK*, et al.* Network diffusion modeling predicts neurodegeneration in traumatic brain injury. Ann Clin Transl Neurol 2020.
Povlishock JT, Katz DI. Update of neuropathology and neurological recovery after traumatic brain injury. J Head Trauma Rehabil 2005; 20(1): 76-94.
Rosenfeld JV, Maas AI, Bragge P, Morganti-Kossmann MC, Manley GT, Gruen RL. Early management of severe traumatic brain injury. Lancet 2012; 380(9847): 1088-98.

Ross DE, Ochs AL, Seabaugh JM, Demark MF, Shrader CR, Marwitz JH*, et al.* Progressive brain atrophy in patients with chronic neuropsychiatric symptoms after mild traumatic brain injury: a preliminary study. Brain Inj 2012; 26(12): 1500-9.
Schott JM, Bartlett JW, Barnes J, Leung KK, Ourselin S, Fox NC*, et al.* Reduced sample sizes for atrophy outcomes in Alzheimer's disease trials: baseline adjustment. Neurobiol Aging 2010; 31(8): 1452-62, 62 e1-2.
Scott G, Zetterberg H, Jolly A, Cole JH, De Simoni S, Jenkins PO*, et al.* Minocycline reduces chronic microglial activation after brain trauma but increases neurodegeneration. Brain 2018; 141(2): 459-71.
Sidaros A, Engberg AW, Sidaros K, Liptrot MG, Herning M, Petersen P*, et al.* Diffusion tensor imaging during recovery from severe traumatic brain injury and relation to clinical outcome: a longitudinal study. Brain 2008; 131(Pt 2): 559-72.
Smith DH, Chen XH, Pierce JE, Wolf JA, Trojanowski JQ, Graham DI*, et al.* Progressive atrophy and neuron death for one year following brain trauma in the rat. J Neurotrauma 1997; 14(10): 715-27.
Smith DH, Johnson VE, Stewart W. Chronic neuropathologies of single and repetitive TBI: substrates of dementia? Nat Rev Neurol 2013; 9(4): 211-21.
Smith SM, Jenkinson M, Johansen-Berg H, Rueckert D, Nichols TE, Mackay CE*, et al.* Tract-based spatial statistics: voxelwise analysis of multi-subject diffusion data. Neuroimage 2006; 31(4): 1487-505.
Strich SJ. Diffuse degeneration of the cerebral white matter in severe dementia following head injury. J Neurol Neurosurg Psychiatry 1956; 19(3): 163-85.
Tagge CA, Fisher AM, Minaeva OV, Gaudreau-Balderrama A, Moncaster JA, Zhang XL*, et al.* Concussion, microvascular injury, and early tauopathy in young athletes after impact head injury and an impact concussion mouse model. Brain 2018; 141(2): 422-58.
Trivedi MA, Ward MA, Hess TM, Gale SD, Dempsey RJ, Rowley HA*, et al.* Longitudinal changes in global brain volume between 79 and 409 days after traumatic brain injury: relationship with duration of coma. J Neurotrauma 2007; 24(5): 766-71.
Tu T-W, Williams RA, Lescher JD, Jikaria N, Turtzo LC, Frank JA. Radiological–pathological correlation of diffusion tensor and magnetization transfer imaging in a closed head traumatic brain injury model. Annals of Neurology 2016; 79(6): 907-20.
Vargas ME, Barres BA. Why is Wallerian degeneration in the CNS so slow? Annu Rev Neurosci 2007; 30: 153-79.
Warner MA, Marquez de la Plata C, Spence J, Wang JY, Harper C, Moore C*, et al.* Assessing spatial relationships between axonal integrity, regional brain volumes, and neuropsychological outcomes after traumatic axonal injury. J Neurotrauma 2010; 27(12): 2121-30.
Wechsler D. WASI: Wechsler Abbreviated Scale of Intelligence. San Antonio, TX: The Psychological Corporation; 1999.
Winkler AM, Ridgway GR, Webster MA, Smith SM, Nichols TE. Permutation inference for the general linear model. Neuroimage 2014; 92: 381-97.
Zanier ER, Bertani I, Sammali E, Pischiutta F, Chiaravalloti MA, Vegliante G*, et al.* Induction of a transmissible tau pathology by traumatic brain injury. Brain 2018; 141(9): 2685-99.
Zhang H, Avants BB, Yushkevich PA, Woo JH, Wang S, McCluskey LF*, et al.* High-dimensional spatial normalization of diffusion tensor images improves the detection of white matter differences: an example study using amyotrophic lateral sclerosis. IEEE Trans Med Imaging 2007; 26(11): 1585-97.

Figure Legends

Figure 1. Neuroimaging analysis pipeline. (A) Diffusion MRI analysis pipeline to generate MNI-space white matter FA map for voxelwise statistics. (B) Volumetric analysis to generate white and grey matter tissue maps from baseline and follow up imaging, with longitudinal registration producing annualized map of change (JD rate change map) for each voxel and a midpoint average image between baseline and follow-up scans. Grey and white matter segmentations are generated, with midpoint average images multiplied by JD maps to generate tissue specific atrophy rates. All images are normalized to MNI space. (C) Voxelwise statistics assessing relationship between baseline FA and brain volume change over time (JD). Summary measures such as mean white matter FA and mean white matter JD used in linear regression.

Figure 2. Evidence of diffuse axonal injury after moderate-severe traumatic brain injury using diffusion MRI. (A) Box plot showing differing mean white matter FA values between patients and controls at baseline and follow-up study visits. (B) Voxelwise contrast of white matter FA values between patients and controls. Areas of significant difference [$P < 0.05$, threshold free cluster enhancement (TFCE) multiple comparison correction] are in red, overlaid on mean FA in green.

Figure 3. Brain volume changes on serial MRI after moderate-severe traumatic brain injury. (A) Box plots showing elevated longitudinal atrophy rates after TBI in grey matter (GM), white matter (WM) and whole brain (WB) tissue classes. All comparisons are statistically significant ($P < 0.001$). (B) Voxelwise map comparing baseline brain volumes after TBI with healthy controls. Areas of significantly lower volume in patients (TFCE multiple comparisons corrected, $P < 0.05$) are shown in red-yellow colour for white matter, blue-light blue for grey matter. (C) Voxelwise map comparing longitudinal atrophy rates (JD maps) after TBI and in healthy controls. Regions of significantly elevated longitudinal atrophy rates are shown in separate colours for different tissue classes. Red-yellow colours indicate white matter regions of significant longitudinal atrophy, whereas blue-light blue colours denote grey matter regions with longitudinal significant atrophy.

Figure 4. Relationship of diffuse axonal injury to atrophy over time. (A) White matter integrity versus atrophy plot. *Z*-scored white matter (WM) FA, quantifying DAI, plotted against JD, quantifying longitudinal atrophy. The green area is hypothesized to include healthy controls (HC) with an undamaged white matter and minimal atrophy. The red region is hypothesized to include TBI patients, with evidence of DAI that correlates with progressive

atrophy. (**B**) *Z*-scored white matter FA plotted against mean white matter JD rate (healthy controls blue, TBI red). (**C**) Voxelwise relationship between baseline FA and JD showing regions where low JD rate is significantly associated with reduced FA (in red $P < 0.05$, TFCE overlaid on mean FA skeleton in green. (**D**) The relationship between zFA and zJD atrophy rate is shown for the peak voxel from analysis (**C**), within the body of the corpus callosum.

Figure 5. White matter damage and atrophy over time across tracts after traumatic brain injury. The relationship between axonal damage (z-scored FA) and atrophy over time (z-scored JD) is shown across white matter regions derived from the Johns Hopkins University White Matter Atlas. Tracts with more evidence of axonal damage show more atrophy, most prominent within large central structures such as the corpus callosum, corona radiata, and internal capsules (adjusted R2 = 0.13, P = 0.0117).

Figure 6. Longitudinal brain atrophy and poorer memory performance after TBI. The relationship between longitudinal atrophy in grey matter (*left*) and white matter (*right*) and a measure of memory at the follow-up visit (the People Test total score) is shown, with significant correlation in each tissue class.

Figure 1.

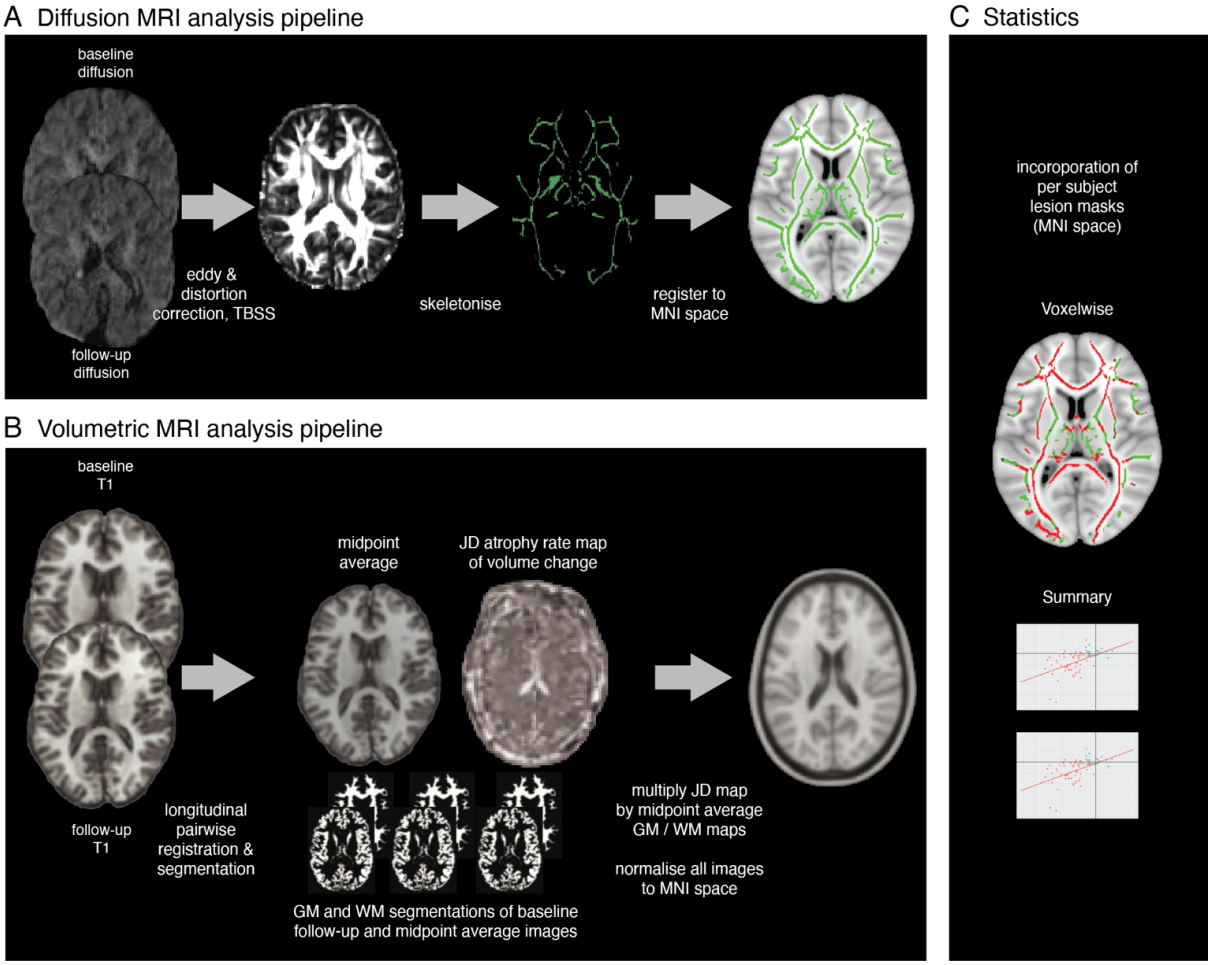

Figure 2.

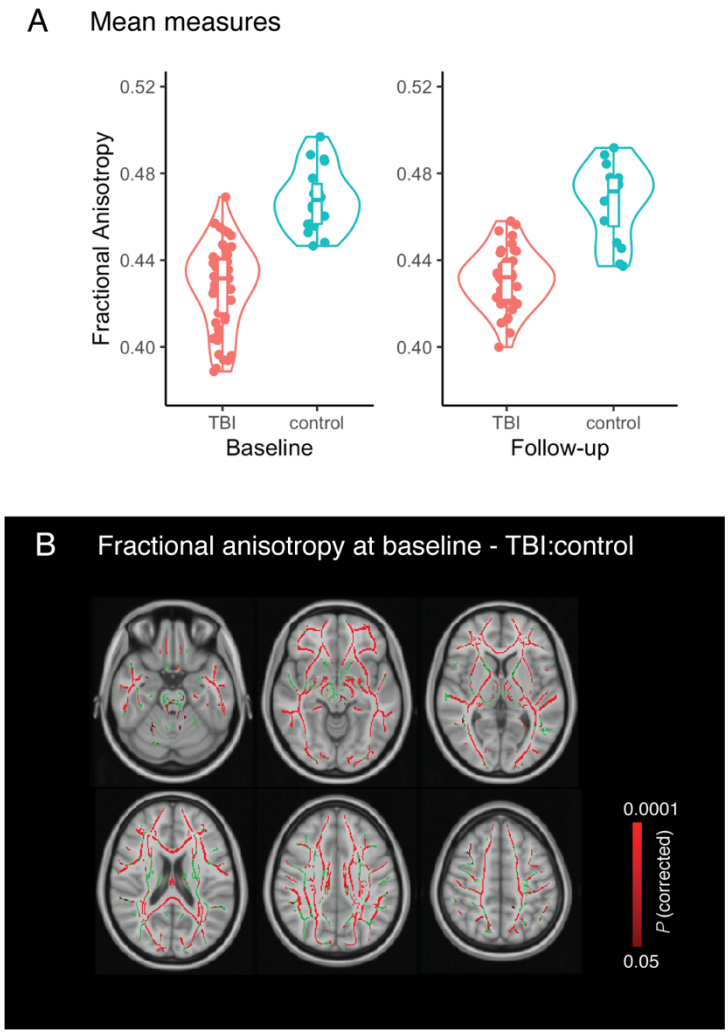
A
Mean measures
Fractional Anisotropy
0.52
0.48
0.44
0.40
TBI
control
Baseline
Follow-up
B
Fractional anisotropy at baseline - TBI:control
0.0001
P (corrected)
0.05

Figure 3

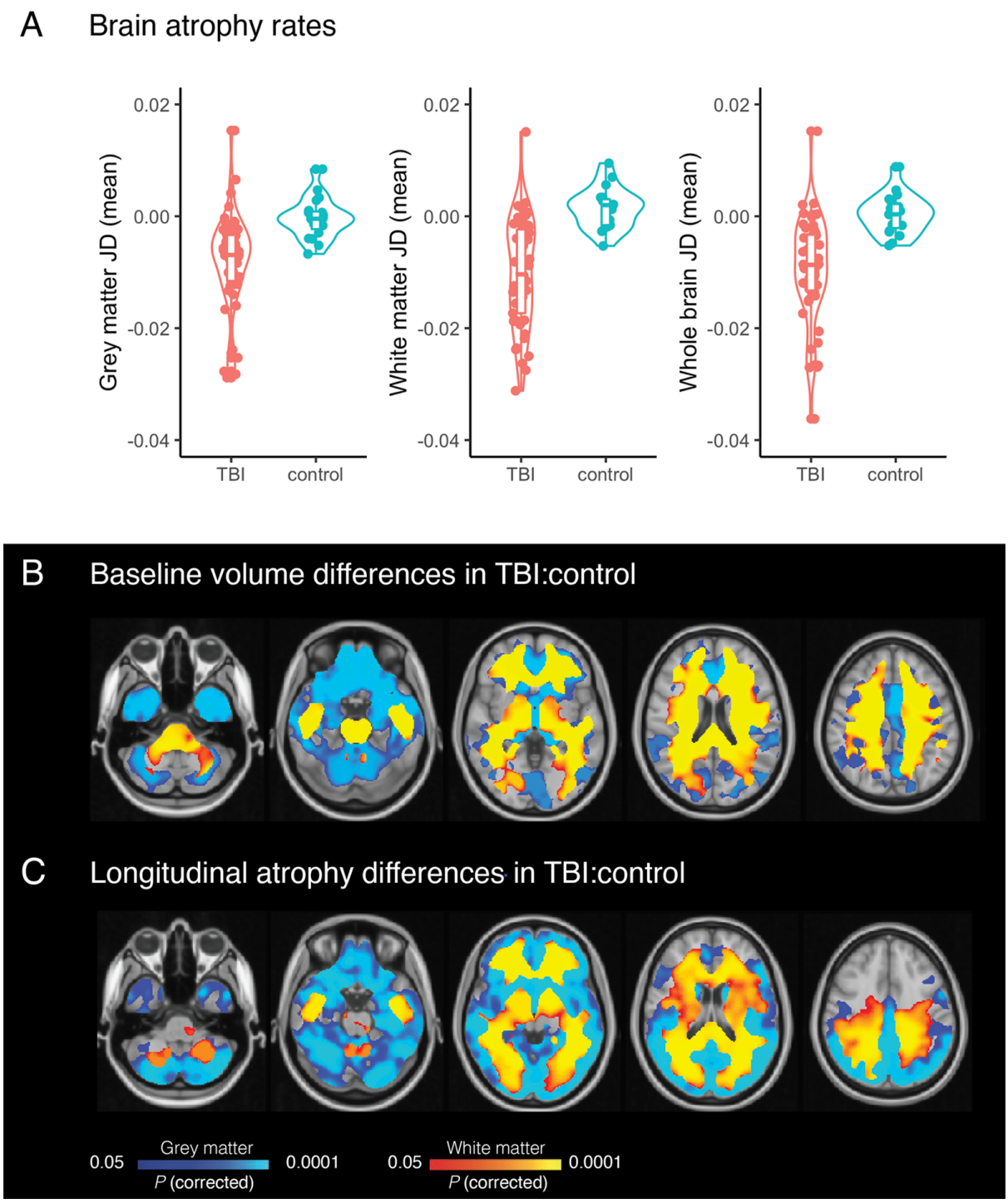
A
Brain atrophy rates
Grey matter JD (mean)
White matter JD (mean)
Whole brain JD (mean)
0.02
0.00
-0.02
-0.04
TBI
control
B
Baseline volume differences in TBI:control
C
Longitudinal atrophy differences in TBI:control
0.05
Grey matter
P (corrected)
0.0001
0.05
White matter
P (corrected)
0.0001

Figure 4

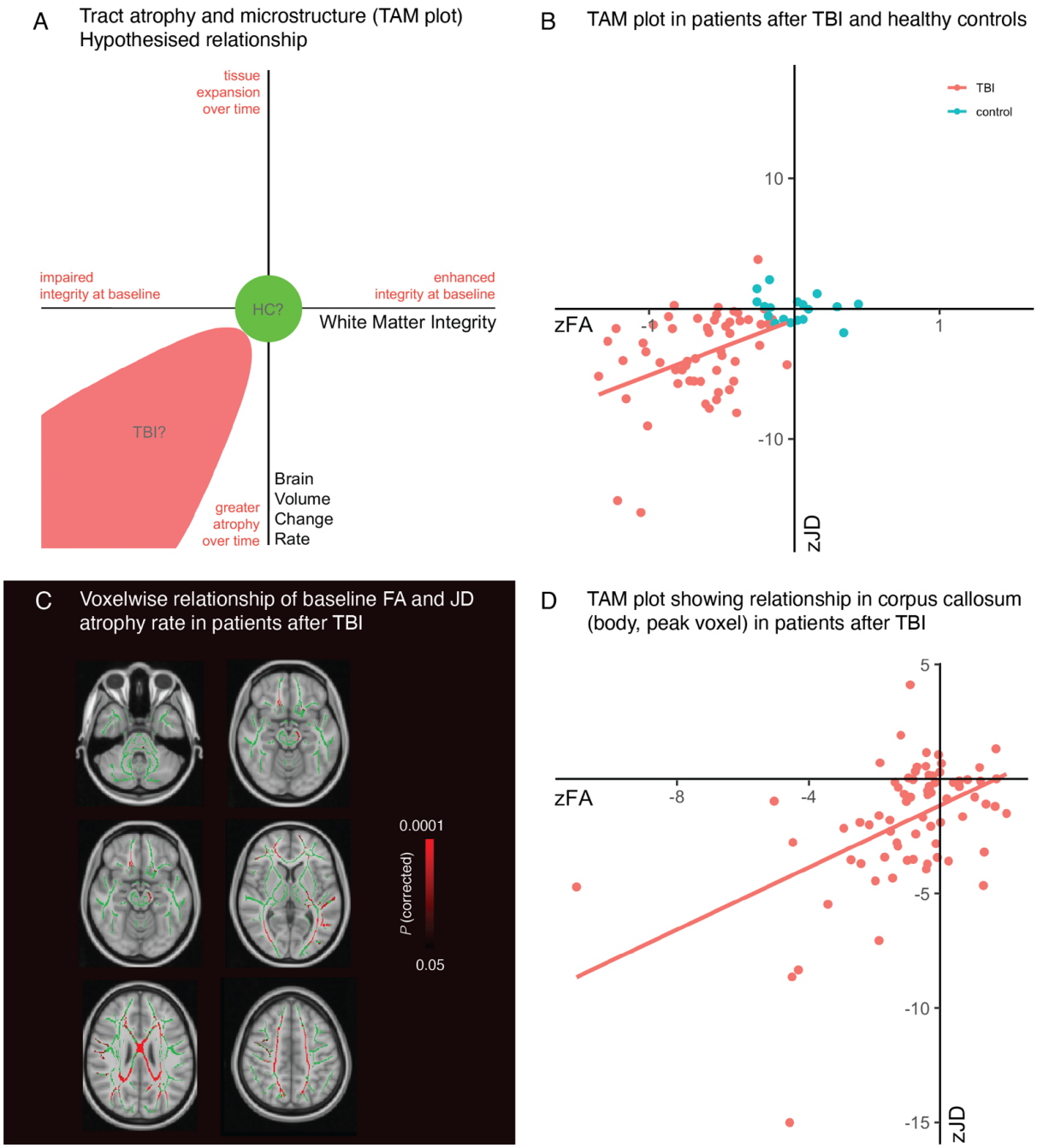
A
Tract atrophy and microstructure (TAM plot)
Hypothesised relationship
tissue expansion over time
impaired integrity at baseline
HC?
enhanced integrity at baseline
White Matter Integrity
TBI?
greater atrophy over time
Brain Volume Change Rate
B
TAM plot in patients after TBI and healthy controls
TBI
control
10
zFA
-1
1
-10
zJD
C
Voxelwise relationship of baseline FA and JD atrophy rate in patients after TBI
0.0001
P (corrected)
0.05
D
TAM plot showing relationship in corpus callosum (body, peak voxel) in patients after TBI
5
zFA
-8
-4
-5
-10
-15
zJD

Figure 5

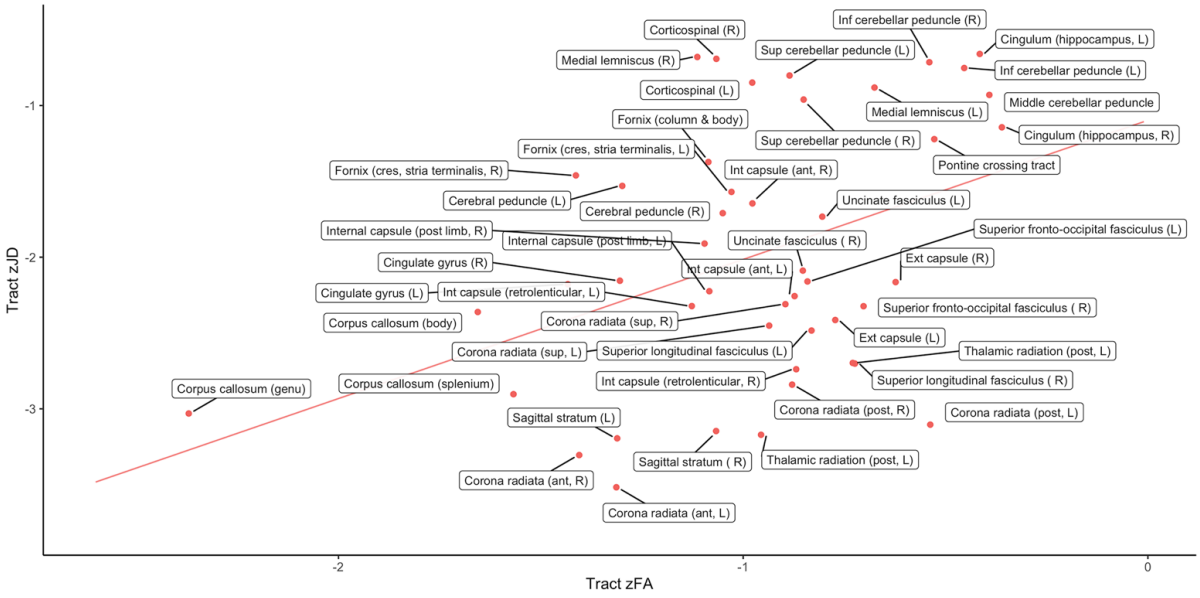
Tract zJD
Tract zFA
-1
-2
-3
-2
-1
0
Corticospinal (R)
Medial lemniscus (R)
Inf cerebellar peduncle (R)
Sup cerebellar peduncle (L)
Cingulum (hippocampus, L)
Inf cerebellar peduncle (L)
Corticospinal (L)
Medial lemniscus (L)
Middle cerebellar peduncle
Fornix (column & body)
Sup cerebellar peduncle (R)
Cingulum (hippocampus, R)
Fornix (cres, stria terminalis, L)
Pontine crossing tract
Fornix (cres, stria terminalis, R)
Int capsule (ant, R)
Cerebral peduncle (L)
Cerebral peduncle (R)
Uncinate fasciculus (L)
Internal capsule (post limb, R)
Internal capsule (post limb, L)
Uncinate fasciculus (R)
Superior fronto-occipital fasciculus (L)
Cingulate gyrus (R)
Int capsule (ant, L)
Ext capsule (R)
Cingulate gyrus (L)
Int capsule (retrolenticular, L)
Corpus callosum (body)
Corona radiata (sup, R)
Superior fronto-occipital fasciculus (R)
Ext capsule (L)
Corona radiata (sup, L)
Superior longitudinal fasciculus (L)
Thalamic radiation (post, L)
Corpus callosum (genu)
Corpus callosum (splenium)
Int capsule (retrolenticular, R)
Superior longitudinal fasciculus (R)
Corona radiata (post, R)
Corona radiata (post, L)
Sagittal stratum (L)
Sagittal stratum (R)
Thalamic radiation (post, L)
Corona radiata (ant, R)
Corona radiata (ant, L)

Figure 6

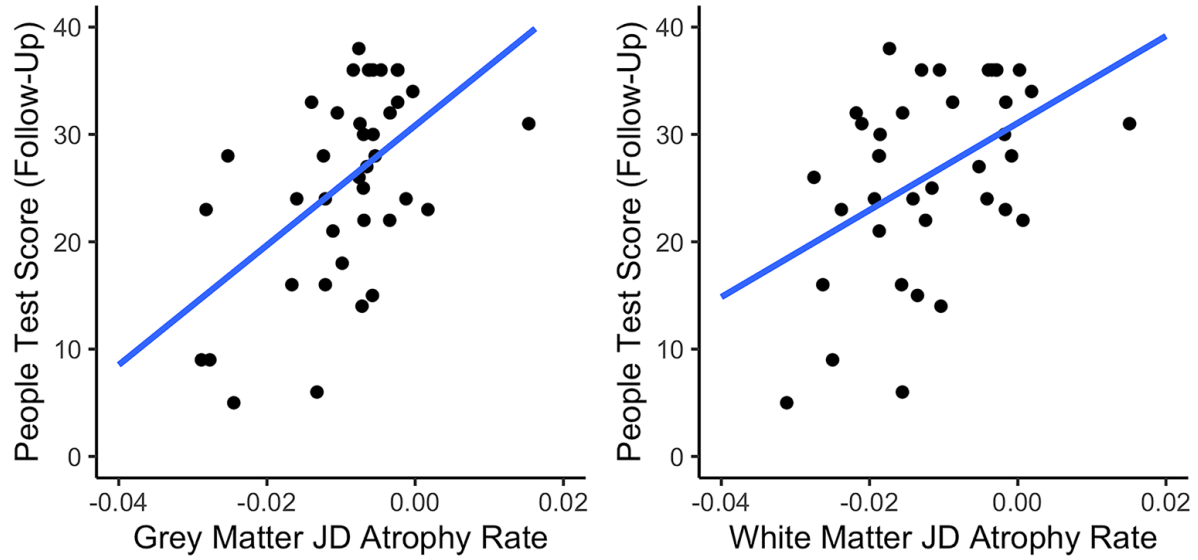
People Test Score (Follow-Up)
Grey Matter JD Atrophy Rate
White Matter JD Atrophy Rate
0
10
20
30
40
-0.04
-0.02
0.00
0.02

Supplementary Material

METHODS

MRI Acquisition Parameters

The following Siemens T1-FE parameters were used: slice thickness = 1.2mm, 150 slices, matrix = 208x208, repetition time = 9.60ms, echo time = 4.60ms, flip angle = 8 degrees, FOV = 24x24cm. For the Philips MPRAGE sequence, slice thickness = 1mm, 160 slices, matrix = 256 x 240, repetition time = 2300ms, echo time = 2.98ms, flip angle = 9 degrees, FOV = 25.6cm x 24cm.

DWI was acquired on the Siemens scanner with the following parameters: Echo time = 103ms, repetition time = 9500ms, 64 contiguous slices, FOV 256mm, voxel size $2mm^3$, b = 1000 s/mm^3, four images with b = 0 s/mm^2. The following parameters were used on the Philips scanner: Voxel size = 1.75 x 1.75 x 2mm, b = 1000 s/mm^3, four images b = 0 s/mm^2, slice thickness = 2mm, 73 contiguous slices, FOV 224mm.

RESULTS

Cross-sectional comparisons stratified by scanner system

To assess for a possible effect of scanner system on cross-sectional results, fractional anisotropy, grey matter, white matter and whole-brain volumes were compared between TBI patients (on each scanner) and controls. Comparisons were performed between the controls and patients from each scanner at baseline, and follow-up. Comparisons of FA, GM, WM and WB volumes remained highly significant when the TBI group was split by scanner at baseline and follow up ($P<0.0001$), except in the case of for baseline GM volume on the Philips system, which was borderline ($P=0.0507$).

Supplementary Figure 1. Focal lesion distribution after moderate-severe TBI

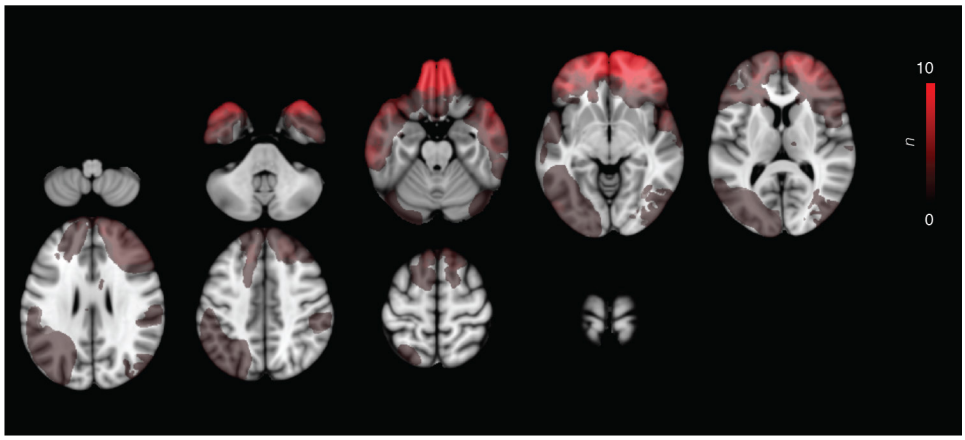

Composite lesion overlay map using red colour bar demonstrating highest lesion density frontally and at the temporal poles. Abbreviations: n = number of cases.

Supplementary Figure 2. Interscan-intervals and white matter atrophy rates

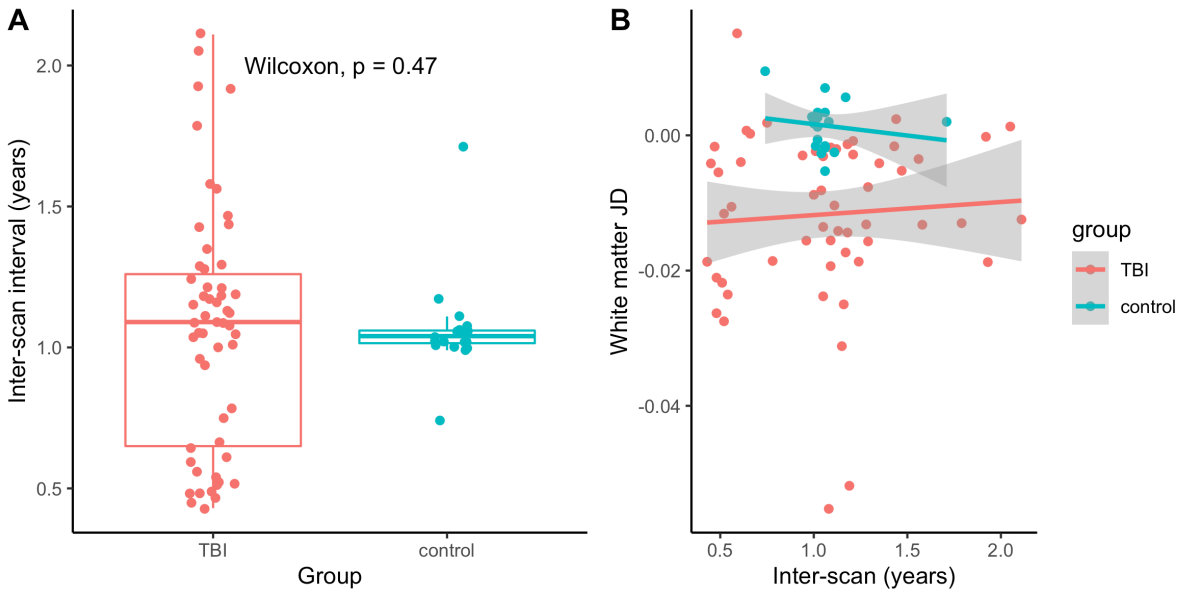

Left plot (A) - distribution of inter-scan intervals (in years) in patients after TBI and healthy controls. There are no significant differences between group means (P=0.47. Right plot (B) - linear regression showing no significant correlations between inter-scan interval and white matter atrophy rate (JD) in either TBI patients or healthy controls (TBI adjusted R^2 -0.01, P

0.63; Control adjusted R^2 -0.03, P=0.50). Patient subgroup analysis based on inter-scan interval did not reveal any significant relationship.

Supplementary Figure 3. Time since injury and white matter atrophy rates in patients after TBI

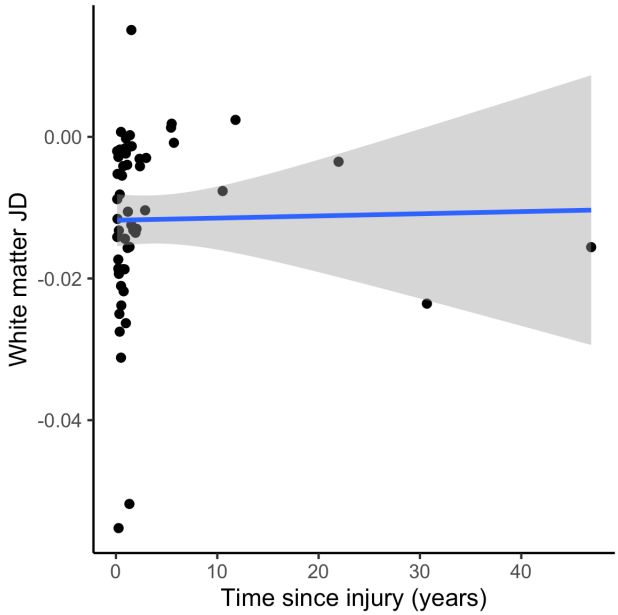

White matter JD atrophy rate in patients do not show any significant correlation with time since injury in patients after moderate-severe TBI (adjusted R^2 -0.02, P=0.89).

Supplementary Table 1. Hierarchical partitioning of variance in FA:JD model

Characteristic	**Independent Variance Explained (%)**
Baseline white matter FA	53.4
Scanner system	33.4
Presence of focal lesion	4.0
Baseline white matter volume	3.8
Time since injury	2.0
Age at baseline scanning visit	1.8
Sex	1.6

Supplementary Table 2. Neuropsychological performance and brain atrophy rates after TBI

	Baseline	Follow-up	Change
People Test Total Score			
n	50	40	37
mean ± SD	23.72 ± 7.86	25.73 ± 9.07	1.86 ± 8.28
WM Jacobian determinant	ρ = 0.28, p = 0.0457*	ρ = 0.53, p = 0.0005**	ρ = 0.29, p = 0.0867
GM Jacobian determinant	ρ = 0.32, p = 0.0252*	ρ = 0.54, p = 0.0004**	ρ = 0.25, p = 0.134
Trails B minus A			
n	50	40	37
mean ± SD	34.52 ± 26.01	33.78 ± 26.73	0.39 ± 30.21
WM Jacobian determinant	ρ = -0.15, p = 0.3079	ρ = -0.26, p = 0.0984	ρ = -0.02, p = 0.8826
GM Jacobian determinant	ρ = -0.12, p = 0.4037	ρ = -0.21, p = 0.1971	ρ = -0.05, p = 0.7878
Choice Reaction Time (median)			
n	42	16	15
mean ± SD	0.49 ± 0.11	0.55 ± 0.11	0.00 ± 0.17
WM Jacobian determinant	ρ = -0.22, p = 0.1642	ρ = 0.2, p = 0.4523	ρ = 0.25, p = 0.3613
GM Jacobian determinant	ρ = -0.14, p = 0.3735	ρ = 0.14, p = 0.6062	ρ = 0.19, p = 0.506
WASI Similarities			
n	30	20	19
mean ± SD	36.27 ± 4.86	34.35 ± 6.13	-0.47 ± 7.11
WM Jacobian determinant	ρ = 0.39, p = 0.0341*	ρ = 0.04, p = 0.8765	ρ = -0.17, p = 0.4808
GM Jacobian determinant	ρ = 0.45, p = 0.0118	ρ = 0.07, p = 0.7828	ρ = -0.2, p = 0.419

** significant at p<0.05; ** significant after false discovery rate (FDR) multiple comparisons correction for 18 independent comparisons; WM: white matter, GM: grey matter*